

## Templated Self-Assembly of Ultrathin Gold Nanowires by Nanoimprinting for Transparent Flexible Electronics

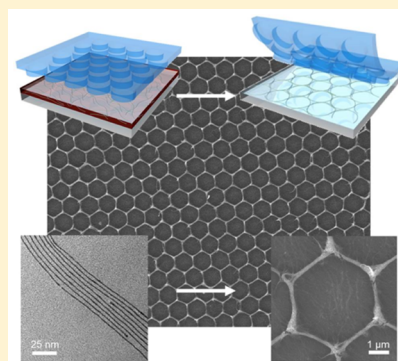
Johannes H. M. Maurer, Lola González-García,\* Beate Reiser, Ioannis Kanelidis, and Tobias Kraus\*

INM—Leibniz Institute for New Materials, Campus D2 2, 66123 Saarbrücken, Germany

### Supporting Information

**ABSTRACT:** We fabricated flexible, transparent, and conductive metal grids as transparent conductive materials (TCM) with adjustable properties by direct nanoimprinting of self-assembling colloidal metal nanowires. Ultrathin gold nanowires (diameter below 2 nm) with high mechanical flexibility were confined in a stamp and readily adapted to its features. During drying, the wires self-assembled into dense bundles that percolated throughout the stamp. The high aspect ratio and the bundling yielded continuous, hierarchical superstructures that connected the entire mesh even at low gold contents. A soft sintering step removed the ligand barriers but retained the imprinted structure. The material exhibited high conductivities (sheet resistances down to 29  $\Omega$ /sq) and transparencies that could be tuned by changing wire concentration and stamp geometry. We obtained TCMs that are suitable for applications such as touch screens. Mechanical bending tests showed a much higher bending resistance than commercial ITO: conductivity dropped by only 5.6% after 450 bending cycles at a bending radius of 5 mm.

**KEYWORDS:** Metal grids, nanoimprint, ultrathin gold nanowires, transparent conductive electrodes, flexible electronics



Transparent conductive electrodes (TCE) are crucial components of modern electronic devices: thin-film displays, solar cells, touch screens, and smart windows, for example. The range of available materials that combine high optical transparency and good electrical conductivity is limited because high carrier concentrations generally imply strong optical absorption. Transparent oxides such as indium tin oxide (ITO) combine both properties and are widely used as TCE.<sup>1</sup> The ceramic brittleness and high temperature vacuum deposition of such oxides impede their application in flexible devices and organic electronics, which motivates the search for a next generation of TCEs.

Metals are promising candidates that combine high electrical conductivity and mechanical elasticity. They are opaque in bulk, but spaced grids of very fine metal structures can provide high transparency at low sheet resistances.<sup>2,3</sup> The geometry of the grid that strongly affects its optical and electrical properties can be optimized for particular applications. It is possible, for example, to design stretchable grids and create flexible TCEs.<sup>4</sup> Transparent metal grids have so far been fabricated using e-beam lithography,<sup>5</sup> nanoimprint lithography,<sup>5</sup> nanosphere lithography,<sup>6</sup> and transfer printing,<sup>7</sup> among others. It is desirable to print TCEs in scalable processes that do not require vacuum; this is possible using solution-based processes based on liquid ink. Table 1 gives an overview of published methods that use metal nanoparticle inks to obtain ordered, transparent, and conductive metal grids for TCEs.

The table demonstrates that TCEs can be printed from solution with high transparency and low sheet resistance. However, the lines of most printed grids are several micron

wide, which necessitates large pitches to attain transparency. Organic solar cells, OLEDs, and ultrahigh definition displays do not perform well with such TCEs.<sup>20,21</sup> In addition, most methods in Table 1 use thermal sintering in order to remove organic ligands and obtain conductivity, thus exceeding the thermal budget of many polymer substrates. Kwon et al. reduced the pitch and prepared silver honeycomb meshes with submicron lines using nanosphere lithography, but their method requires multiple processing steps and is limited to a specific geometry.<sup>17</sup>

Here, we introduce a single-step patterning process that creates highly transparent, conductive, and flexible metal grid electrodes with submicron lines by directly nanoimprinting colloidal ink. The method relies on the extreme anisotropy and flexibility of chemically prepared ultrathin nanowires and their ability to form hierarchical superstructures by self-assembly.

Direct nanoimprint of colloidal inks combines the advantages of solution processing (low thermal budget, simple equipment) with the advantages of nanoimprinting (high resolution and scalability)<sup>22</sup> and has been used to arrange spherical nanoparticles into plasmonic structures<sup>23,24</sup> and electrical circuits.<sup>25–28</sup> For transparent electronics, anisotropic particles are favorable. Particles with high aspect ratios reduce the percolation threshold and the number of tunnel barriers at particle–particle interfaces, enhancing the performance of the printed TCE significantly.<sup>29,30</sup> It is challenging, however, to

**Received:** October 23, 2015

**Revised:** January 27, 2016

**Published:** March 17, 2016

**Table 1. Overview of Different Liquid-Based Methods to Produce Ordered Metal Grids Based on Nanoparticle Inks for TCEs and Properties of the Fabricated Materials**

method	material	line width ( $\mu\text{m}$ )	pitch ( $\mu\text{m}$ )	line height (nm)	resistivity ( $\mu\Omega\text{ cm}$ )	$\rho_{\text{material}}/\rho_{\text{bulk}}$	sheet resistance ( $\Omega/\text{sq}$ )	transmittance (%)	sintering conditions	ref
direct writing	Ag	9	100–400	3000	36.5–122	23–77		77.4–94.1	2 h/200–350 °C	8
EHD jet printing	Ag	7.53	50–300	1460	78.2	49	1–18	67–86.7	30 min/200 °C NIR	9
	Ag	13–82	250–750				1–7	60–84.2	20 min/180 °C	10
laser sintering	Ag	10–30	200–500	130	7	4.4	6–30	75–91		11
	Ni	6.5	10–500	35–40	63	9	40–5000	39–97		12
inkjet + coffee ring	Ag	5–10	800–900	600–800	57–261	36–164		91.2	2 h/160–200 °C	13
	Ag	5–10	150	<300	43–51	27–32	4	95	HCl vapor	14
evaporative lithography	Au	4	100	80			20	82	20 min/425 °C	15
	Ag	5.7	50	1123	$\approx 10$	6.3	9	77	30s/HCl vapor	16
nanosphere lithography	Ag	0.05–0.5	3	70–200			30–2000	35–71	5 min/100 °C	17
		0.3	10	222			20–35	82.6–88	+ 10 min/140 °C	
PDMS wrinkles	Ag	10–20	65–36				2.9–29	74.6–88.6	20 min/200 °C	18
flow-coating	Ag	7–10.6	200	60	30–180	19–113	132–332	70–88	1 h/150 °C	19

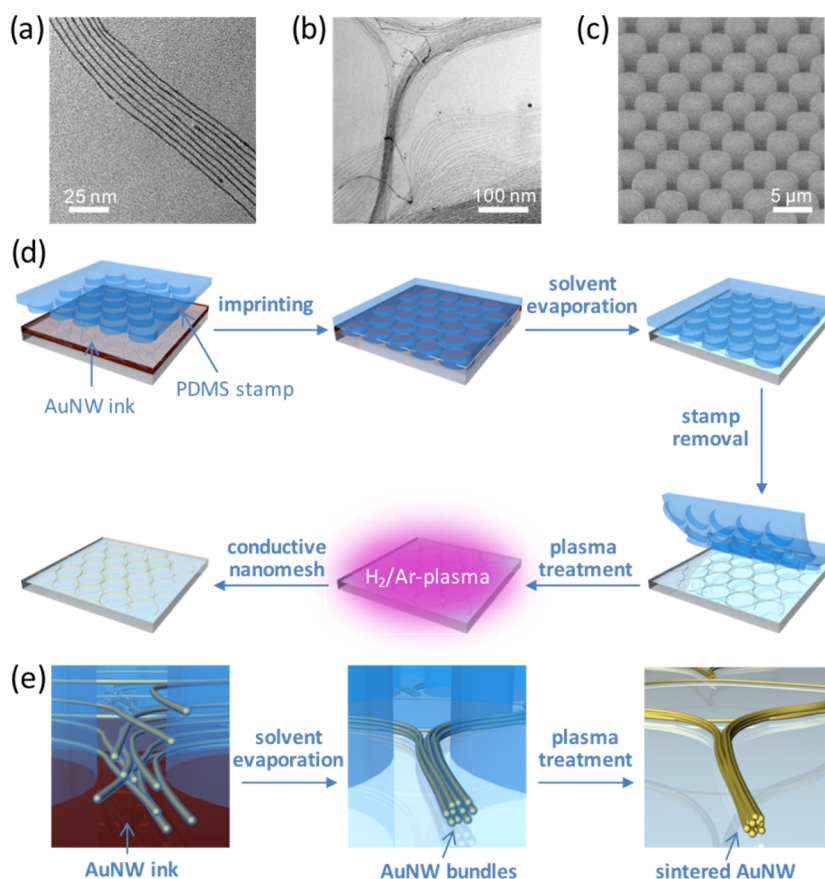


**Figure 1.** (a, b) Transmission electron micrographs of as-synthesized ultrathin gold nanowires. Bundles of interdigitating wires are formed during drying. (c) Scanning electron micrograph of used PDMS pillar structure. (d) Schematic diagram of the nanoimprinting process, which consists of the following steps: 1. spreading of the AuNW ink on a substrate; 2. imprinting using a PDMS stamp; 3. evaporation of the solvent; 4. removal of the stamp; 5. plasma treatment of the imprinted structure. (e) Detailed schematic diagram of the bundling and sintering process.

pattern anisotropic nanoparticles with nanoimprint: if the wires are long and rigid, they will not follow the large curvatures of small grids.

Here, we show that extremely thin gold wires that are highly bendable solve the problem and provide ideal inks for the nanoimprint of metal grids. Ultrathin gold nanowires have diameters around 1.6 nm, aspect ratios above 1000, and can be prepared in a simple, fast, and scalable synthesis (Figure 1a).<sup>31,32</sup> Gold provides superior stability against chemical degradation compared to other metals. Their extremely high

aspect ratio causes percolation at relatively low concentration and lends them great mechanical flexibility.<sup>33,34</sup> We observed bending radii down to 20 nm without breakage in TEM (Figure S1, Supporting Information). The wires readily follow nanoscale features of a stamp. AuNWs tend to self-assemble into bundles, a spontaneous process that occurs during solvent evaporation and eases the formation of percolating networks over macroscopic distances (Figure 1b).<sup>31,35</sup> The bundles can be sintered by a gentle plasma treatment to remove insulating

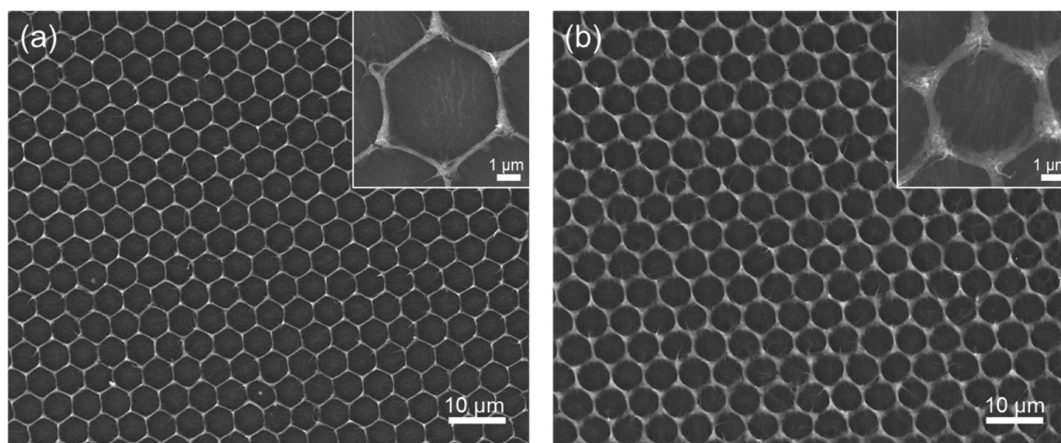


**Figure 2.** SEM images of imprinted gold nanowires after plasma treatment for (a) low concentration (NM-15 nm) and (b) high concentration (NM-45 nm) of nanowires. Insets show magnifications of bundled nanowires after sintering.

oleylamine capping ligand and form stable superstructures, as reported in our previous work.<sup>32</sup>

Nanoimprint of AuNWs does not require vacuum processing, it is amenable to large-scale production, and provides compatibility with polymer substrates. The complete process is performed at room temperature, and the patterning is achieved in a single imprinting step. Figure 1d illustrates our process. A drop of AuNWs in cyclohexane is dispensed on a substrate. A polydimethylsiloxane (PDMS) stamp is placed onto the liquid and makes conformal contact with the substrate. AuNWs are confined in the cavities, and the solvent starts evaporating through the stamp. During solvent evaporation, AuNWs interconnect like a yarn made of wool fibers and form continuous, hierarchical superstructures that readily follow the stamp geometry, building the final mesh structure. The width and height of the superstructures, and thus, of the final mesh lines, depends on the concentration of nanowires in the ink for a given stamp geometry. Higher concentration implies more wires in the stamp cavities, which leads to the formation of larger bundles and to thicker and wider lines. In contrast to conventional nanoimprint, the final mesh lines are always considerably smaller than the stamp features, because the solid content of the AuNW ink is below 100%. The lower limits are set by the minimal wire concentration required to create percolation during solvent evaporation. Because the bundling process occurs during drying, the nanowires keep their mobility and flexibility during the patterning process, which allows the shaping of complex geometries. After complete solvent evaporation, the stamp can be removed. The bundled wires are then sintered by a hydrogen plasma (5% hydrogen in argon) at room temperature into a stable and conductive mesh.<sup>32</sup> Figure 1e shows a detailed schematic diagram of the bundling and sintering process. We used a stamp that carried a hexagonal array of pillars with diameters of 4 μm, a pitch of 5 μm, and a pillar height of 5 μm (Figure 1c) to obtain hexagonal networks of AuNW bundles further referred as nanomeshes (NMs, see Figure 2). The process is not limited to this geometry, of course, and it is easy to create arbitrary structures via photolithography and PDMS molding.

Variation of the AuNW concentration led to changes in line thickness and width. Atomic force microscopy (AFM) measurements of the sintered nanomeshes revealed an average line thickness of 15 nm and a minimum width of around 250 nm for a concentration of 4 mg/mL (NM-15 nm, Figure 2a)

and an average thickness of 45 nm and a minimum width of 600 nm for 8 mg/mL (NM-45 nm, Figure 2b).

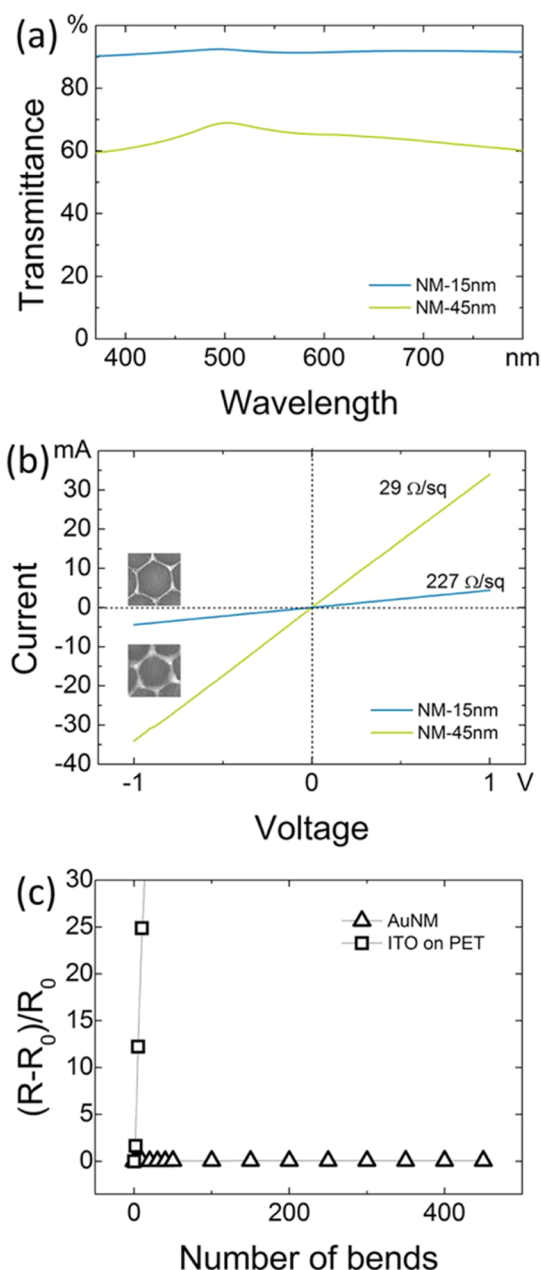
Figure 3a shows the optical transmittance of the sintered gold nanomeshes. The thinner mesh (NM-15 nm) had a very high ballistic optical transmittance (92% at 500 nm) over the entire visible range. The thicker gold mesh (NM-45 nm) had an optical transmission of 68% at 500 nm. Both values are in good agreement with values calculated using simple geometric models: the clear aperture of the mesh is defined as the fraction of surface that is not covered by gold. It is directly proportional to the optical transmittance according to geometrical optics, which predicts transmittances of 90% for the thin mesh and 70% for the thick mesh. The experimental values slightly vary, probably due to diffuse scattering and interference at the grid that are not considered in our simple calculation.<sup>3</sup> The average haze was measured to be 1.6% (NM-15 nm) and 2.7% (NM-45 nm), respectively, which is in the range required for displays (<3%).<sup>36</sup>

Figure 3b shows the current–voltage characteristics of the sintered meshes. Both exhibited ohmic conductance with sheet resistances of 227 Ω/sq for NM-15 nm and 29 Ω/sq for NM-45 nm. For comparison, random nanowire films with a thickness of 10 nm had an average transmittance of 66% and sheet resistances up to 50 Ω/sq. Thinner random films with higher transmittance (compared to NM-15 nm) were not conductive, because the required annealing step led to decomposition of the wires and loss of percolation for such ultrathin films.<sup>32</sup>

Based on Kirchoff's rules, the sheet resistance of a regular metal grid equals

$$R_s = \frac{\rho d}{wh} \quad (1)$$

where  $\rho$  is the resistivity,  $d$  is the network pitch,  $w$  is the line width, and  $h$  is the height of the grid.<sup>21</sup> The bulk resistivity of gold ( $2.44 \times 10^{-8}$  Ω m) gives theoretical sheet resistances of 32.5 Ω/sq for the thin mesh ( $d = 5$  μm,  $w = 250$  nm,  $h = 15$  nm) and 4.5 Ω/sq for the thick mesh ( $d = 5$  μm,  $w = 600$  nm,  $h = 45$  nm). The resistance of both meshes was approximately 7 times this limit, which is in the range expected for electrodes based on sintered nanoparticle inks (see also Table 1).<sup>8,9,11,12</sup> Conductivity is limited by a combination of structural grid defects, grain boundary scattering, nanopores, and variations of the line width.<sup>3</sup>



**Figure 3.** (a) Optical ballistic transmittance spectra and (b) current–voltage curves for both samples. (c) Averaged normalized change in resistance  $(R - R_0)/R_0$  for nanoimprinted gold nanomeshes (AuNMs) and ITO on PET as a function of bending cycles under tension. The bending curvature was 5 mm.

The mechanical flexibility and the effect of bending on conductivity were tested with gold nanomeshes imprinted on PET substrates that initially had an average sheet resistance of  $100 \text{ } \Omega/\text{sq}$ . Figure 3c shows the mean variation in sheet resistance  $(R - R_0)/R_0$  as a function of bending cycles for the imprinted nanomeshes compared to a commercially available ITO film on PET (Sigma-Aldrich,  $R_0 = 100 \text{ } \Omega/\text{sq}$ ). The samples were bent under tension with a bending radius of 5 mm. The resistance of the ITO films increased by several orders of magnitude after a few bending cycles. We tested 10 of our meshes and consistently found an increase in resistance that was below 1 order of magnitude within the first 50 bends,

followed by an asymptotic trend that reached  $(R - R_0)/R_0 = 0.056$  in average after 450 bends.

The results demonstrate that AuNW nanoimprinting yields transparent, conductive, and flexible grid electrodes with submicron lines and small pitch. The values of transparency and sheet resistance obtained were in the range typically required for TCEs.<sup>2</sup> Lower sheet resistances are possible by increasing the height of the printed lines. The small height of below 50 nm is desirable for thin film organic solar cells and OLEDs. The versatility of our new method opens the door for custom designs, and we expect further improvements on the electrode performance with tailored grid geometry.

In summary, we showed that the mechanical flexibility of AuNWs and their self-assembly behavior make them suitable components for nanoimprinting inks. Percolation and electrical conductivity occur at particle concentrations far below those required for inks of spherical particles.<sup>30</sup> The spontaneous bundling of AuNW naturally leads to superstructures with bending-resistant conductivity. Because it occurs during drying, bundling does not impede the imprinting process.

The final, imprinted structure consists of bundled AuNWs that follow the predefined pattern of the stamp. There are large overlaps between the ultrathin wires in the bundles enabling percolation throughout the grid pattern. This bundling simplifies annealing. Gentle plasma processing at room temperature is sufficient to remove the insulating ligand and sinter them together to create a highly conductive grid.

The pivotal properties of the wires, high mechanical flexibility and self-assembly, are not intrinsic properties of gold but are governed by the geometry of the wires and the ligand's solvation. We believe that this process can be applied to ultrathin nanowires made of various materials. Protocols are available for ultrathin semiconductor and platinum nanowires.<sup>37</sup>

We have only just begun to explore this combination of self-assembly and templating; surface modification of stamps and substrates and other nanowire ligands should provide more control. Future, hierarchical printing processes could combine self-assembly (controlled by microscopic features of the stamp) with macroscopic patterning of electronic circuits. This would allow tuning material properties locally and integrating them in functional devices in a single step.

**Experimental Section.** *AuNW Synthesis.* Ultrathin gold nanowires were synthesized as described in previous work.<sup>31,32</sup> In a typical synthesis, 39 mg of  $\text{HAuCl}_4 \cdot 3\text{H}_2\text{O}$  were dissolved in a mixture of 5.8 mL of *n*-hexane (99%, ABCR, Germany) and 1.7 mL of oleylamine (technical grade, 70%, Sigma-Aldrich, Steinheim, Germany). 1.5 mL of triisopropylsilane (98%, ABCR, Germany) were added and the solution was kept undisturbed at RT overnight. The wires were precipitated by adding ethanol. The supernatant was removed, and the wires were redispersed in *n*-hexane. The washing step was repeated once, and the wires were finally redispersed in cyclohexane to achieve gold concentrations of 4 and 8 mg/mL, respectively.

*Fabrication of PDMS Stamps.* The PDMS stamp was prepared using a lithographically fabricated silicon master (size  $1 \times 1 \text{ cm}^2$ ). The prepolymer and the cross-linker of a PDMS kit (Sylgard 184, Dow Corning) were mixed in a 10:1 weight ratio and degassed until no air bubbles were visible. The mixture was then poured on the silicon master, which had been silanized with a trichloro(octadecyl)silane (Sigma-Aldrich, St. Louis, MO, USA) before, and fully cured at  $70 \text{ } ^\circ\text{C}$ . After that, the PDMS was peeled off the master. We used a stamp that carried

a hexagonal array of pillars with diameters of 4  $\mu\text{m}$ , a pitch of 5  $\mu\text{m}$ , and a pillar height of 5  $\mu\text{m}$ .

**Nanoimprinting.** 30  $\mu\text{L}$  of the AuNW dispersion in cyclohexane was dropped onto a glass microscope slide or PET foil, respectively, and the stamp was immediately placed on top. After complete solvent evaporation, the stamp was removed. Plasma treatment was performed in a RF PICO plasma system (Diener electronic, Ebhausen, Germany) operating at 0.3 mbar gas pressure and 100 W RF (13.56 MHz) power using mixture of 5% hydrogen in argon for 15 min.

**Characterization.** TEM images were acquired to characterize the single AuNWs using a JEM 2010 (JEOL, Germany) operating at 200 kV. SEM images were recorded using a Quanta 400 ESEM (FEI, Germany). AFM measurements were recorded using a NanoWizard3 (JPK Instruments, Germany). Optical characterization was performed by UV–vis spectroscopy in transmission mode (Cary 5000, Varian). The bare glass substrate was taken as baseline. Total transmittance in the visible light spectrum (400–800 nm) was measured with an integrating sphere, and the haze of the material was calculated as the ratio between the diffusive transmittance (difference in total transmittance ( $T_{\text{tot}}$ ) and ballistic transmittance ( $T_{\text{ball}}$ )) and the total transmittance ( $T_{\text{tot}}$ ):

$$\text{haze} = (T_{\text{tot}} - T_{\text{ball}})/T_{\text{tot}} \times 100 \quad (2)$$

Current–voltage ( $I$ – $V$ ) measurements were performed using a Keithley 2450 sourcemeter. For the flexibility test, the gold nanomeshes on PET were bent under tension around a steel rod with a radius of 5 mm; conductivity was measured in the flat state.

## ■ ASSOCIATED CONTENT

### ● Supporting Information

The Supporting Information is available free of charge on the ACS Publications website at DOI: 10.1021/acs.nanolett.5b04319.

TEM image of bent ultrathin gold nanowires (PDF)  
Movie S1 (AVI)

## ■ AUTHOR INFORMATION

### Corresponding Authors

\*E-mail: lola.gonzalez-garcia@leibniz-inm.de.

\*E-mail: tobias.kraus@leibniz-inm.de.

### Notes

The authors declare no competing financial interest.

## ■ ACKNOWLEDGMENTS

The authors would like to thank Eduard Arzt for his continuing support of the project. The authors thank Sarah Fischer for providing PDMS templates and Roland Bennewitz for the access to the AFM. Funding from the German Federal Ministry of Education and Research in the “NanoMatFutur” program is gratefully acknowledged.

## ■ REFERENCES

- (1) Ellmer, K. *Nat. Photonics* **2012**, *6* (12), 809–817.
- (2) Layani, M.; Kamysny, A.; Magdassi, S. *Nanoscale* **2014**, *6* (11), 5581–5591.
- (3) Van De Groep, J.; Spinelli, P.; Polman, A. *Nano Lett.* **2012**, *12* (6), 3138–3144.
- (4) Kim, D. H.; Rogers, J. A. *Adv. Mater.* **2008**, *20* (24), 4887–4892.

- (5) Kang, M.-G.; Guo, L. J. *Adv. Mater.* **2007**, *19* (10), 1391–1396.
- (6) Gao, T.; Wang, B.; Ding, B.; Lee, J.-K.; Leu, P. W. *Nano Lett.* **2014**, *14* (6), 3694.
- (7) Kang, M.-G.; Joon Park, H.; Hyun Ahn, S.; Jay Guo, L. *Sol. Energy Mater. Sol. Cells* **2010**, *94* (6), 1179–1184.
- (8) Ahn, B. Y.; Lorang, D. J.; Lewis, J. A. *Nanoscale* **2011**, *3* (7), 2700–2702.
- (9) Jang, Y.; Kim, J.; Byun, D. *J. Phys. D: Appl. Phys.* **2013**, *46*, 155103.
- (10) Park, J.; Hwang, J. *J. Phys. D: Appl. Phys.* **2014**, *47*, 405102.
- (11) Hong, S.; Yeo, J.; Kim, G.; Kim, D.; Lee, H.; Kwon, J.; Lee, H.; Lee, P.; Ko, S. H. *ACS Nano* **2013**, *7* (6), 5024–5031.
- (12) Lee, D.; Paeng, D.; Park, H. K.; Grigoropoulos, C. P. *ACS Nano* **2014**, *8* (10), 9807–9814.
- (13) Zhang, Z.; Zhang, X.; Xin, Z.; Deng, M.; Wen, Y.; Song, Y. *Adv. Mater.* **2013**, *25* (46), 6714–6718.
- (14) Layani, M.; Gruchko, M.; Milo, O.; Balberg, I.; Azulay, D.; Magdassi, S. *ACS Nano* **2009**, *3* (11), 3537–3542.
- (15) Higashitani, K.; McNamee, C. E.; Nakayama, M. *Langmuir* **2011**, *27* (6), 2080–2083.
- (16) Layani, M.; Magdassi, S. *J. Mater. Chem.* **2011**, *21* (39), 15378.
- (17) Kwon, N.; Kim, K.; Sung, S.; Yi, I.; Chung, I. *Nanotechnology* **2013**, *24* (23), 235205.
- (18) Wu, H.; Menon, M.; Gates, E.; Balasubramanian, A.; Bettinger, C. J. *Adv. Mater.* **2014**, *26* (5), 706–711.
- (19) Park, J. H.; Lee, D. Y.; Seung, W.; Sun, Q.; Kim, S.-W.; Cho, J. H. *J. Phys. Chem. C* **2015**, *119* (14), 7802–7808.
- (20) Kang, M. G.; Kim, M. S.; Kim, J. S.; Guo, L. J. *Adv. Mater.* **2008**, *20* (24), 4408–4413.
- (21) Neyts, K.; Real, A.; Marescaux, M.; Mladenovski, S.; Beeckman, J. *J. Appl. Phys.* **2008**, *103* (9), 093113.
- (22) Ahn, S. H.; Guo, L. J. *Adv. Mater.* **2008**, *20* (11), 2044–2049.
- (23) Liang, C.-C.; Liao, M.-Y.; Chen, W.-Y.; Cheng, T.-C.; Chang, W.-H.; Lin, C.-H. *Opt. Express* **2011**, *19* (5), 4768–4776.
- (24) Fafarman, A. T.; Hong, S.-H.; Caglayan, H.; Ye, X.; Diroll, B. T.; Paik, T.; Engheta, N.; Murray, C. B.; Kagan, C. R. *Nano Lett.* **2013**, *13* (2), 350–357.
- (25) Ko, S. H.; Park, I.; Pan, H.; Grigoropoulos, C. P.; Pisano, A. P.; Luscombe, C. K.; Fréchet, J. M. J. *Nano Lett.* **2007**, *7* (7), 1869–1877.
- (26) Park, I.; Ko, S. H.; Pan, H.; Grigoropoulos, C. P.; Pisano, A. P.; Fréchet, J. M. J.; Lee, E.-S.; Jeong, J.-H. *Adv. Mater.* **2008**, *20* (3), 489–496.
- (27) Yu, X.; Pham, J. T.; Subramani, C.; Creran, B.; Yeh, Y.-C.; Du, K.; Patra, D.; Miranda, O. R.; Crosby, A. J.; Rotello, V. M. *Adv. Mater.* **2012**, *24* (47), 6330–6334.
- (28) Hu, P.; Li, K.; Chen, W.; Peng, L.; Chu, D.; O’Neill, W. J. *Micromech. Microeng.* **2010**, *20* (12), 129802.
- (29) Mutiso, R. M.; Sherrott, M. C.; Rathmell, A. R.; Wiley, B. J.; Winey, K. I. *ACS Nano* **2013**, *7* (9), 7654–7663.
- (30) Kumar, S. K.; Krishnamoorti, R. *Annu. Rev. Chem. Biomol. Eng.* **2010**, *1* (1), 37–58.
- (31) Feng, H.; Yang, Y.; You, Y.; Li, G.; Guo, J.; Yu, T.; Shen, Z.; Wu, T.; Xing, B. *Chem. Commun.* **2009**, 1984–1986.
- (32) Maurer, J. H. M.; González-García, L.; Reiser, B.; Kanelidis, I.; Kraus, T. *ACS Appl. Mater. Interfaces* **2015**, *7*, 7838–7842.
- (33) Sánchez-Iglesias, A.; Rivas-Murias, B.; Grzelczak, M.; Pérez-Juste, J.; Liz-Marzán, L. M.; Rivadulla, F.; Correa-Duarte, M. A. *Nano Lett.* **2012**, *12* (12), 6066–6070.
- (34) Chen, Y.; Ouyang, Z.; Gu, M.; Cheng, W. *Adv. Mater.* **2013**, *25* (1), 80–85.
- (35) Loubat, A.; Impéror-Clerc, M.; Pansu, B.; Meneau, F.; Raquet, B.; Viau, G.; Lacroix, L.-M. *Langmuir* **2014**, *30* (14), 4005–4012.
- (36) Kim, T.; Canlier, A.; Cho, C.; Rozyyev, V.; Lee, J.; Han, S. M. *ACS Appl. Mater. Interfaces* **2014**, *6* (16), 13527–13534.
- (37) Cademartiri, L.; Ozin, G. A. *Adv. Mater.* **2009**, *21* (9), 1013–1020.